EULERIAN AND LAGRANGIAN ASPECTS OF OCEANIC ROSSBY DYNAMICS

S. Pierini and E. Zambianchi
Istituto di Meteorologia e Oceanografia, Università di Napoli Parthenope
Via A. De Gasperi, 5 – 80133 Napoli - Italy

Abstract

In this paper the Rossby dynamics, which is one of the main aspects of the oceanic wind-driven variability, is reviewed, and the Lagrangian chaos associated with Rossby waves in a closed domain is discussed in order to put in evidence Rossby wave transport properties.

A discussion of the basic features of planetary and topographic, barotropic and baroclinic Rossby waves is presented. Evidence of the relevance baroclinic planetary waves have in shaping the wind-driven response of large oceans, both at mid and low latitudes, is given by discussing data obtained recently by the TOPEX/POSEIDON altimeter. As far as the Mediterranean Sea is concerned, modeling results are shown supporting the possibility that barotropic planetary Rossby wave variability be present in the western basin. The discrete spectrum associated with the Rossby dynamics in a closed domain is then considered. Numerical results concerning the Strait of Sicily and the Iceland-Faeroe ridge are presented as examples of topographic Rossby normal modes. Laboratory modeling of such dynamical features performed in the large "Coriolis" rotating tank in Grenoble is also discussed.

We then pass to consider an analytical model for Rossby normal modes in a circular domain, and the Lagrangian chaos associated with these motions. The Poincaré maps of the evolution of an initial patch of particles show the different degree of Lagrangian chaos for different amplitudes of the flow and the classical stirring and folding of material lines. The first normal mode leads to a strong mixing in the direction of phase propagation while the second mode produces a stronger dispersion in the normal direction. A quantitative analysis of chaotic advection is carried out by computing in several relevant cases the particle pair correlation function H and the Finite Size Lyapunov Exponent, yielding that such a mechanism may contribute significantly to tracer dispersion in basins characterized by the presence of Rossby normal modes.

I. INTRODUCTION

The time-dependent dynamics of large-scale subinertial motions in the atmosphere and oceans is shaped by Rossby waves (also known as planetary waves, PRWs). They are quasigeostrophic, baroclinic or barotropic rotational waves whose existence derives from the conservation of potential vorticity of fluid columns in an ambient in which planetary vorticity varies with latitude (the so-called beta-effect). In the atmosphere Rossby waves constitute the basic dynamical feature of mid-latitude weather patterns. In the ocean they provide the mechanism for the adjustment to the large

scale atmospheric forcing. More specifically, oceanic Rossby waves play a fundamental role in phenomena such as the westward intensification of the wind-driven gyres, the oceanic response to large scale fluctuating winds, boundary current radiation, etc.. A topographical counterpart of planetary Rossby waves exists in the form of "topographic" Rossby waves (TRWs), particularly important in oceanography, for which the variable ambient vorticity is provided by strong variations of the fluid depth. Moreover, the continuous Rossby wave spectrum typical of horizontally unbounded domains is complemented by a discrete spectrum of planetary or topographic Rossby normal modes (PRMs, TRMs), associated to closed or semi-closed areas.

In this paper Eulerian and Lagrangian aspects of the oceanic Rossby dynamics are considered. We begin by presenting an overview of some relevant examples of planetary Rossby waves (section 2) and topographic Rossby waves and modes (section 3), based on observational, modeling and laboratory studies in a Eulerian framework. In section 4 a specific analytical solution of the quasigeostrophic equation representing forced Rossby waves and modes is discussed, and a discussion of the associated chaotic advection (considered as a prototype of Rossby wave Lagrangian dispersion properties) is finally presented in section 5.

II. PLANETARY ROSSBY WAVES

As mentioned in the introduction, Rossby waves are solutions of the so-called quasigeostrophic equation, which can be derived from the equation of conservation of potential vorticity in the shallow-water approximation under the assumption of subinertial motions. Consideration of the general theory of Rossby waves goes beyond the scope of this paper: the interested reader not familiar with this topic can refer to classical and exhaustive text-books in the oceanographic context, such as those of Le Blond and Mysak (1978), Gill (1982), and Pedlosky (1987; 1996). In section 4, however, detailed reference is made to a particular Rossby wave problem that will be studied also from a Lagrangian point of view in section 5. Here we limit ourselves to remind the dispersion relation for Rossby waves on the mid-latitude β-plane in a 2-layer system:

$$\omega = \frac{-\beta k_x}{k_x^2 + k_y^2 + R^{-2}} \tag{2.1}$$

where ω is the angular frequency, $\mathbf{k} = (k_x, k_y)$ is the horizontal wave-number, x and y are aligned along a parallel and a meridian respectively, $\beta = (2\Omega_{earth}/R_{earth})\cos\varphi$ is the derivative of the Coriolis parameter $f = 2\Omega_{earth}\sin\varphi$ with respect to latitude (Ω_{earth} is the earth angular velocity, R_{earth} is the earth radius and φ is the latitude), $R = R_e = \sqrt{g\,(D_1 + D_2)}/f$ is the external Rossby deformation radius for barotropic waves and $R = R_i = \sqrt{g'\bar{D}}/f$ is the internal Rossby deformation radius for baroclinic waves (where g is the acceleration of gravity, $g' = g\Delta\rho/\rho$ is the "reduced gravity", $\Delta\rho/\rho$ is the relative variation of density in the two layers, D_1 and D_2 are the depths of the two layers, and $\bar{D} = D_1 D_2/\,(D_1 + D_2)$). From (2.1) follows that, for zonal wave-numbers (k_y=0), the phase velocity $c_p = \omega/k_x$ is always westward oriented while the group velocity (in the absence of mean flow) $c_g = d\omega/dk_x$ is westward for $k_x < R^{-1}$ but eastward for $k_x > R^{-1}$.

Planetary Rossby waves in large oceans have recently been revealed with unprecedented accuracy, spatial extension and resolution from altimeter missions, in particular from the most recent ones TOPEX/POSEIDON (T/P) and ERS 1-2. Since for Rossby waves the geostrophic balance between the Coriolis force and the horizontal pressure gradient force holds, the dynamically active sea surface height signal (obtained from the altimeter data after subtraction of the steric height, tidal and inverted barometer signals) allows one to derive the subsurface currents associated to them (e.g., Robinson, 1994; Pierini, 2002a). Perhaps the most striking example of Rossby wave observations with T/P altimeter data is provided by Chelton and Schlax (1996), but several other analyses of the same nature have been carried out (e.g., Polito and Cornillon, 1997; Maltrud et al., 1998; White et al., 1998; Döös, 1999; Vivier et al., 1999; Witter and Gordon, 1999; Cipollini et al., 2000; Kobashi and Kawamura, 2001).

The study of Chelton and Schlax (1996) provides an excellent overview of salient features of baroclinic planetary Rossby waves (with periods above 3 months) as observed from T/P altimeter data. Alternating positive and negative sea level signals with a clear sign of westward propagation are evident over most of the world oceans. The observed frequencies span over a range $\approx$0.5-2 cpy. The propagating signals account for $\approx$30% of the total variance at $\varphi<15^\circ$ and for $\approx$10% of the total variance at $\varphi>30^\circ$ (at sufficiently high latitudes baroclinic Rossby waves cannot exist because (2.1) yields a cutoff frequency at $k=R^{-1}$). Baroclinic Rossby waves appear to originate mainly from the eastern boundary, where local wind and buoyancy forcings may account for part of their energy, but Rossby wave radiation as a consequence of the passage of poleward traveling Kelvin waves generated at low latitudes is also an important (perhaps the predominant) generating mechanism (Pierini, 2003). In the tropical belt (but outside the equatorial waveguide, which is centered at the equator and embraces a latitudinal belt of few degrees) weak westward penetration is found, associated with a particular spatial structure known as beta-refraction pattern (e.g., White, 1977; Schopf et al., 1981; Philander, 1990). This phenomenon is due to the refraction toward the equator of low latitude baroclinic Rossby wave packets originating from the eastern coast, for which the zonal group velocity (of O (10 cm/s)) increases with decreasing latitude as φ^{-2}. A recent model study (Pierini, 2003) of seasonally varying refraction patterns has obtained a validation from the spatially integrated T/P altimeter observations of Stammer (1997). In the equatorial waveguide equatorial Rossby waves (e.g. Gill, 1982) are found to travel westward with a speed of O (100 cm/s). For both mid-latitude and equatorial Rossby waves the phase speed in the west exceeds that in the east of up to $\approx$50% because of the deepening of the thermocline in the west (associated with the baroclinic compensation of the subtropical gyre equatorward return flow in the oceanic interior), which implies a larger D_1, and thus a larger R_i, in the west than in the east. Rossby waves are found to be generated also in mid-ocean regions mainly because of the interaction of local currents with important topographic features (e.g. the mid-ocean ridge in the North Atlantic or the Hawaiian ridge in the North Pacific). Finally, also open ocean Ekman pumping accounts for Rossby wave generation.

Barotropic Rossby waves are much faster than baroclinic Rossby waves and shape mainly the sub-seasonal barotropic response of the ocean to variable wind stress. They also have been revealed by altimeter data (e.g., Chao and Fu, 1995; Fu and Davidson, 1995; Kobashi and Kawamura, 2001) and, instead of being generated at the eastern boundary at mid and low latitudes (as happens for baroclinic waves, see above discussion) they, on the contrary, appear to be originated at the western boundary at mid and

high latitudes. Pierini (1998b) has interpreted this as the response of a linear-inertial regime in the framework of a more general theory of wind-driven fluctuating western boundary currents, in which a second viscous regime yields westward intensified Sverdrup oscillations of non-propagating character.

Are planetary Rossby waves expected to play a role also in smaller oceanic basins, such as Mediterranean subbasins? For Rossby waves the smaller the spatial scales, the smaller their frequencies (the planetary beta-effect needs a large latitudinal extension to be felt), therefore, in principle, only barotropic PRWs could be expected to be present in the Mediterranean Sea. However, the topographic beta-effect (corresponding to a variable ambient "planetary" vorticity due to topographic variations) was shown to cancel almost everywhere in the Mediterranean Sea the planetary beta-effect. In a numerical process study about the effect of topography on the structure of PRMs in a box (Pierini, 1997) it was shown that the presence of shelf and slope topographies representing larger and larger regions of intense topographic beta-effect leads to a progressive shift to lower frequencies of the lowest Rossby mode (because of the reduced effective length scale of the basin) accompanied by a remarkable reduction of the amplitude at resonance. For large topographic gradients covering more than 90% of the total basin area (in the Mediterranean this represents a typical situation for the Central Ionian and the Tyrrhenian Sea), the existence of planetary modes and even any sign of westward propagation appears to be prevented by the overwhelming action of the topographic steering. On the other hand, regions of very small topographic gradients are present in the Mediterranean Sea (e.g. the Algero-Provençal basin west of Sardinia or the south-western Ionian Sea) for which the existence of PRWs, though modified by the topography, cannot in principle be ruled out. These are results of an idealized process study; now the question arises as to whether the barotropic planetary dynamics is really absent in the Tyrrhenian Sea and if it indeed plays some role in the Algero-Provençal basin, as suggested by these numerical results. Experimental evidence of this would require current meter measurements in the deep sea, not yet available, so at this stage numerical modelling is a valuable tool to investigate this particular aspect of the circulation.

A numerical study was therefore carried out in order to analyze the actual existence of Rossby modes in the Algero-Provençal basin (Pierini, 1998a). The dynamics forced by the "National Meteorological Center" winds was studied in a domain including the Western Mediterranean and part of the Ionian Sea. In order to focus on the part of the flow that is strictly related to the Rossby dynamics -and therefore to the planetary beta-effect- the barotropic shallow-water equations were solved with and without the term βy in the Coriolis parameter and then the difference between the two fields thus obtained was computed (we may denote this field as beta-residual). In the Algero-Provençal basin a relevant beta-residual signal was indeed found, the corresponding transport explaining about 30% of the total wind-driven signal. Episodes of Rossby wave excitation and subsequent free propagation are evident in the Provençal basin after all major wind stress anomalies. In the Tyrrhenian Sea, on the contrary, no planetary Rossby wave activity is present, in agreement with the theoretical arguments described above. An approximate two-month period can be roughly estimated for the main Rossby wave episodes, in agreement with the first Rossby eigenperiod computed for a 400x800 km rectangular domain.

III. TOPOGRAPHIC ROSSBY WAVES AND MODES

In real oceanic basins lateral boundaries and bottom topography can play an important role in several cases. As far as the effect of later boundaries is concerned, multiple reflections at coasts can give rise to PRMs, with a discrete set of eigenperiods dependent on the geometry of the basin. PRMs contribute to shape the very high frequency barotropic variability of large oceans. Willebrand et al. (1980) showed in a numerical study that in the North Atlantic the characteristic time scale of dissipation is larger than the time necessary for barotropic Rossby waves to propagate westward across the basin for the 4-5 lowest basin modes, so that they may be excited, with periods ranging from 10 to 15 days. Pierini (1990, 1997) showed that in fact these modes can be in equilibrium with the wind without any substantial westward intensification, while for higher forcing periods the forced response is in terms of westward intensified Rossby modes (Pierini, 1998b). In the Atlantic Ocean PRMs appear to have never been unambiguously observed while in the Pacific Ocean Luther (1982) showed persuasive evidence of a 4-6 day PRM with an energy e-folding time of less than three days.

As far as topography is concerned, at the end of the preceding section a case was considered (the Tyrrhenian Sea) for which the planetary beta-effect is completely overshadowed by an equivalent topographic beta-effect. Another important dynamical consequence of topography on PRWs that deserves to be mentioned is that associated to the interaction of the waves with a strong topographic variation with isobaths almost normal to the wave-number, such as the Atlantic mid-ocean ridge (e.g., Barnier, 1984; Matano, 1995; Pedlosky and Spall, 1999; Pedlosky, 2000). In other cases the topographic beta-effect can support coherent Rossby waves denoted as topographic Rossby waves (TRWs, e.g. Thompson, 1971, Thompson and Luyten, 1976, Okkonen, 1993). Obviously, these kinds of motions are basically barotropic, because only for them the topographic effect manifests itself in terms of an equivalent beta-effect in the potential vorticity balance (e.g., Pedlosky, 1987). On the other hand, the concurrent effect of topography and lateral boundaries can give rise to topographic Rossby normal modes (TRMs).

TRMs (e.g. Ripa, 1978) are fundamental elements in the theory of long-period tides (e.g. Wunsch, 1967; Platzman et al., 1981; Carton, 1983; Miller et al., 1993), determining locally the structure of the tidal response. However, only recently experimental and numerical evidence was provided suggesting that such dynamical features can play an important role in coastal oceanography. In a study on the circulation over the ridge connecting Iceland to the Faeroe islands, Miller et al. (1996) gave the first experimental evidence of a TRM. Both the experimental eigenperiod 1.8 days and the corresponding spatial structure of the mode were satisfactorily explained by a shallow water model. Pierini (1996) applied a barotropic circulation model to the central Mediterranean Sea and showed that TRMs with periods ranging from 2 to 5 days can be excited in the Strait of Sicily by both wind anomalies and remote barotropic flows produced by pressure fluctuations on a basin scale. Theoretical evidence that TRMs can be excited in the Mediterranean Sea is also provided by Candela and Lozano (1994). In general, because of their small periods, the possible existence of TRMs in several oceanographic sites might not be revealed in residual current signals simply because the modes may be filtered out together with the tidal currents. It is therefore possible that TRMs could be more ubiquitous than is usually believed, also in view of their ability to be excited easily by different forcing agents (Pierini, 1996). As-

sessing this hypothesis would be relevant for the understanding of horizontal mixing in regions of bounded topographic slopes. Sections 4-5 of this paper are devoted to analyzing this aspect.

As far as laboratory studies are concerned, simulations in rotating tanks to model topographic Rossby waves have been carried out, for instance, by Sommeria et al. (1991). Pedlosky and Greenspan (1967) and Beardsley (1975) conducted analytical, laboratory and numerical investigations into the role of TRMs in the "sliced cylinder" model. The combined process of Rossby wave generation, wave reflection at horizontal boundaries and consequent excitation of normal modes in the laboratory has been considered by Pierini et al. (2002), who performed laboratory simulations of TRMs in the large "Coriolis" Rotating Platform in Grenoble following an original approach inspired by numerical simulations carried out in the Sicily Strait (Pierini, 1996). The basic feature of the bottom topography was a linear slope of 4.3x2 m delimited by two lateral walls. Since the studied motions are essentially barotropic, homogeneous water was used. Unsheared currents were generated by a simple movement of a paddle located in front of the topographic barrier. The conservation of potential vorticity for the currents flowing onto the channel slope produced Rossby waves: reflections at the lateral boundaries then led to the formation of propagating barotropic TRMs, whose frequencies and spatial structures were selected by the physical system. The currents were measured every 30 seconds through the Correlation Imaging Velocimetry method, which allowed an extremely detailed synoptic map of the horizontal velocities in an area ($\sim$13 m^2) including the slope. A variety of experiments were performed in order to provide a complete process study in which the effect of different channel lengths and rotation periods could be tested. Two different lengths of the linear slope, 4.3 and 3.3 m, and rotation periods ranging from 30 to 50 sec were considered. The qualitative analysis of the 2D current patterns, and the good agreement found between the measured eigenperiods and the periods obtained by means of a simple analytical model, showed that in all cases the first Rossby normal mode was generated. Moreover, numerical simulations based on the shallow water equations, for a geometry and paddle movements that matched closely the experimental setup, allowed to calibrate the analytical model and provided useful information on a discrepancy found between experimental and analytical eigenperiods due to an oscillation of the normal mode trajectory.

IV. AN ANALYTICAL MODEL FOR FORCED ROSSBY NORMAL MODES

In this section a specific analytical solution of the quasigeostrophic equation of conservation of potential vorticity in terms of Rossby normal modes in a circle will be used to analyze Lagrangian transport properties of Rossby dynamics in a simplified framework. We introduce the following nondimensionalization (dimensional variables are with overbars):

$$(\bar{\mathbf{x}}, \bar{\eta}) = (\mathbf{x}, \eta)\ R, \quad \bar{t} = \frac{t}{\beta R}, \quad \bar{\mathbf{u}} = \mathbf{u}\beta R^2, \quad \bar{\tau} = \frac{\beta \rho g D R}{f_0}\,\tau$$

where **x**=(*x*,*y*) are the horizontal coordinates, **u**=(*u*,*v*) the horizontal velocities, η is the sea surface displacement, *R* the radius of the circle E, *D* the constant water depth, $f = f_0 + \beta y$ the Coriolis parameter, ρ the constant water density, τ the wind stress.

With these positions the linearized quasigeostrophic, divergent equation of conservation of potential vorticity and the geostrophic balance in nondimensional variables read (e.g., Pedlosky, 1987):

$$\begin{cases} \frac{\partial}{\partial t}\left(\nabla^2\eta - \mu\eta\right) + \frac{\partial \eta}{\partial x} = -curl_z\tau \\ \mathbf{u} = \chi\left(-\frac{\partial \eta}{\partial y}, \frac{\partial \eta}{\partial x}\right) \end{cases} \tag{4.1}$$

with the nondimensional parameters μ and χ defined as:

$$\mu = \frac{R^2 f_0^2}{gD}, \quad \chi = \frac{g}{\beta R^2 f_0}$$

(μ is know as the divergence parameter). The boundary conditions complementing problem (4.1) are:

$$\eta|_{\partial E} = C\left(t\right), \quad \frac{d}{dt}\oint\limits_{\partial E} \nabla\eta \cdot \mathbf{n} ds = -\int\limits\int\limits_{E} \mathrm{curl}_z\tau \, d^2x \tag{4.2}$$

where the first expression, in which $C\left(t\right)$ is an unknown function of time, is the free-slip boundary condition and the second one expresses the conservation of mass. We consider a wind stress oscillating with frequency $\bar{\Omega} = \beta R\Omega$, $\tau = \tau_0\left(\mathbf{x}\right) \, e^{-i\Omega t}$, with $\mathrm{curl}_z\tau_0 = const.$ Under these conditions the equilibrium solution of (4.1-2) in polar coordinates (r, θ) is (Pierini, 1990):

$$\eta_\Omega\left(\mathbf{x}, t\right) = \Re e\left\{ i\frac{\mathrm{curl}\tau_0}{\mu\Omega}\left[1 - \frac{\mu}{4\Gamma}\frac{\varphi\left(\Omega, \mathbf{x}\right)}{H\left(\Omega\right)}\right] \mathrm{e}^{-i\Omega t}\right\} \tag{4.3}$$

where

$$\begin{cases} \varphi\left(\Omega, x\right) = \sum\limits_{m=0}^{\infty} \frac{2}{a_m} \, i^m \frac{J_m(1/2\Omega)}{J_m(\Gamma)} J_m\left(\Gamma r\right)\cos\left(m\theta\right) \, e^{-i\frac{r}{2\Omega}\cos\theta} \\ H\left(\Omega\right) = \sum\limits_{m=0}^{\infty} \frac{J_m^2(1/2\Omega)}{a_m}\frac{J_m'(\Gamma)}{J_m(\Gamma)} \\ \Gamma^2 = \frac{1}{4\Omega^2} - \mu, \quad a_m = \begin{cases} 2, & m = 0 \\ 1, & m \geq 1 \end{cases} \end{cases}$$

(J_m are the Bessel functions of the first kind). The homogeneous version of (4.1-2) ($\tau = 0$) admits solutions in the form of Rossby normal modes:

$$\eta_n\left(\mathbf{x}, t\right) = \Re e\left\{\gamma\,\varphi_n\left(\mathbf{x}\right) \, e^{-i\Omega_n t}\right\} \tag{4.4}$$

where γ is an arbitrary constant and the eigenfrequencies and the eigenfunctions φ_n are given by:

$$H\left(\Omega_n\right) = 0, \quad \varphi_n\left(\mathbf{x}\right) = \varphi\left(\Omega_n, \mathbf{x}\right) \tag{4.5}$$

Thus, the equilibrium response (4.3) resonates at the Rossby eigenfrequencies of the system. For $\Omega \approx \Omega_n$, however, solution (4.3) does not provide the amplitude of the response since no limiting mechanisms such as dissipation and nonlinearities are taken into account. In general, in order to represent the intensity of the basic flow we will make use of an average value of the velocity induced at the forcing period $T = 2\pi/\Omega$:

$$\langle |\mathbf{u}| \rangle_T = \frac{1}{\pi T} \iint_E d^2x \int_0^T |\mathbf{u}| \, dt \tag{4.6}$$

For a forcing frequency Ω far from an Ω_n (4.6) provides a direct information about the strength of the basic flow which is more useful than a quantity related to τ_0. If, on the other hand, a normal mode will be considered, the arbitrary constant γ in (4.4) will be set to provide a given $\langle |\mathbf{u}| \rangle$. Figure 1 shows $\langle |\mathbf{u}| \rangle$ versus the forcing period for $\mathrm{curl}\tau_0 = 1$. The first four modes are evident, with periods T_1=30.40, T_2=48.23, T_3=64.68, T_4=69.46.

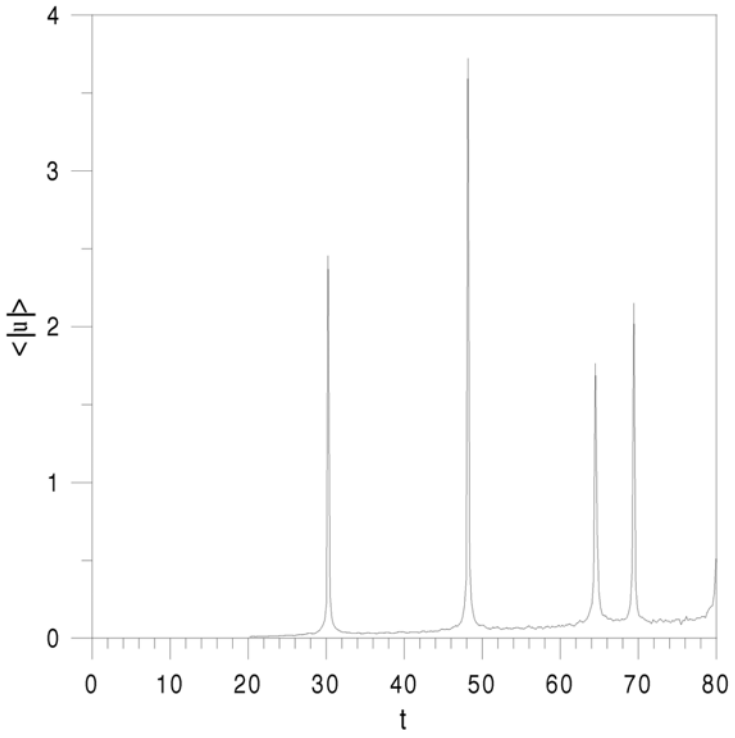

Fig. 1 - Average Eulerian velocity $\langle |\mathbf{u}| \rangle$ versus the forcing period *T* for $\mathrm{curl}\tau_0 = 1$.

The spatial structure of the first two modes is reported in Figure 2a,b. Note the leftward (westward for a planetary mode, for which β>0) propagation typical of the Rossby waves. In a rectangular domain Pedlosky (1987, sect. 3.25) showed that nondivergent Rossby modes can be seen as the superposition of four appropriate Rossby waves all having the same frequency. They can be grouped into two pairs, two *long* and two *short* waves each pair being the result of the reflection of the other pair at the opposite wall. All waves propagate their phase to the west and have the same energy flux.

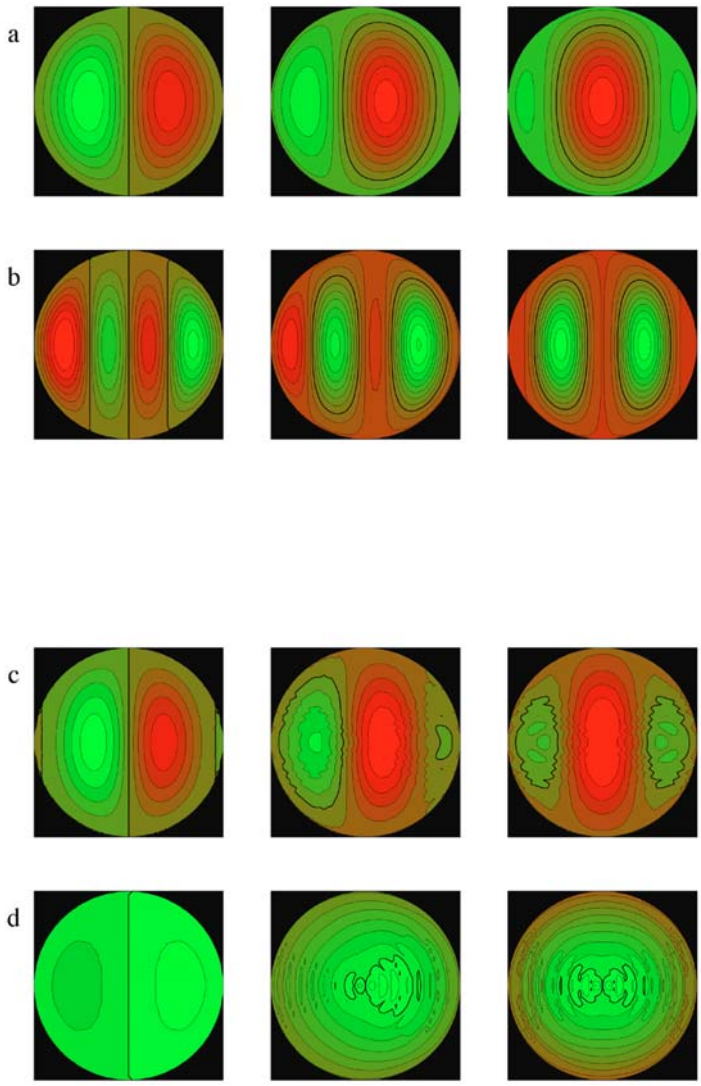

Fig. 2 - Streamfunction of the first mode (a, T=30.40); of the second mode (b, T=48.23); of a mixed first-second mode (c, T=35); of a mixed oscillating boundary layer-first mode (c, T=10). The three snapshots refer to $t = 0, T/8, T/4$.

However, the group velocities of the long waves have a westward component while those of the short waves have an eastward component, in such a way that the sum of the energy flux vectors add to zero, which implies no energy transmission inside the basin. This is, however, a typical Eulerian property which, as we will see, coexists with very complex time, spatial and amplitude-dependent Lagrangian transport properties. Figure 2c shows the forced response at a period between the first and the second mode (T=35), for which an intermediate spatial structure can be recognized. On the contrary, the response shown in Figure 2d corresponding to T=10 is remarkably different from the previous ones. In this case, since the forcing period is smaller than the lowest eigenperiod the propagating character of the flow weakens (being limited in a central portion of the domain) and the response tends, for smaller and smaller periods (but always in the subinertial range) to an oscillatory inertial boundary layer. To this respect it is worth noticing that one of the nice features of solution (2.3) is that it is continuously valid for both $T>T_1$ and $T<T_1$ and, in the latter case, it correctly models the oscillatory boundary layer thanks to its horizontal divergence (Pierini, 1990).

In the applications nondimensional quantities will be used but, in order to consider a realistic situation one can, for example, refer to the dimensional case corresponding to the TRMs obtained in the numerical study concerning the Straits of Sicily (Pierini, 1996). We can choose β=86.4x10^{-11} rad m^{-1}s^{-1}, f_0=0.88x10^{-4} rad s^{-1}, R=150 km, D=1000 m, so that with these parameters the time and velocity scales are $1/\beta R = 7716$ s and $\beta R^2 = 19.44$ m s^{-1} respectively, $\bar{T}_1 = 2.7$ days (the period of the most energetic mode obtained from the numerical simulations) and $\bar{T}_2 = 4.3$ days. Another example is that of the PRMs in the Mediterranean discussed by Pierini (1990) for which β=1.6x10^{-11} rad m^{-1}s^{-1}, f_0=10^{-4} rad s^{-1}, R=500 km, D=2000 m, $1/\beta R = 125000$ s, $\beta R^2 = 4$ m s^{-1}, $\bar{T}_1 = 44$ days and $\bar{T}_2 = 69.8$ days.

V. CHAOTIC ADVECTION PRODUCED BY THE ROSSBY NORMAL MODES

In this section we analyze the chaotic advection produced by the wind-driven flows discussed in section 4. At first, a qualitative analysis of the behaviour of a passive tracer can be carried out on the basis of the Poincaré maps, which describe the evolution of a patch of particles at any given number of cycles. We therefore integrate the trajectory equation for a velocity field given by (4.1) with (4.3) for 1000 particles initially deployed with a regular spacing along a circumference with a radius r=0.33.

We start by considering the first normal mode, whose structure is reported in Fig. 2a. Fig. 3 shows the position of the particles at 3, 6 and 9 cycles for three different amplitudes, $\langle|\mathbf{u}|\rangle = 0.01, 0.05, 0.1$. The first thing to be noticed is the highly nonlinear character of the dispersion produced by the basic flow: while in the first case only a small deformation of the initial patch is produced, a factor 5 in the average Eulerian velocity leads to the typical behaviour of Lagrangian chaos, namely the stretching and folding of material lines associated with the growth of tracer concentration gradients (e.g. Ottino, 1989; Crisanti et al., 1991). A further factor 2 produces an almost complete dispersal of the 1000 particles over the domain already after 6-9 cycles. Even in this case, of course, if a larger number of particles were considered a finer stretching and folding of lines would be observed. The intermediate amplitude case is particularly useful in revealing the anisotropy of the chaotic advection for the first normal

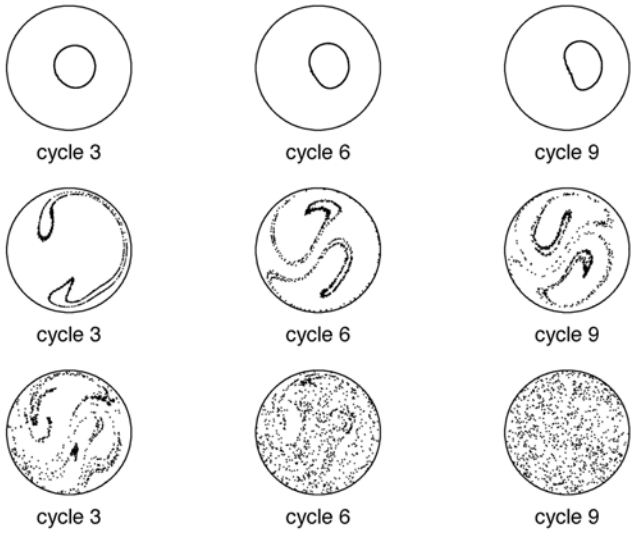

Fig. 3 - Poincaré maps giving the evolved position of 1000 particles initially distributed as in Figure 3. The basic flow is a first normal mode with $\langle|\mathbf{u}|\rangle$=0.01 (upper time sequence), 0.05 (intermediate), 0.1 (lower).

mode. Indeed the evolution from 3 to 6 and 9 cycles evidences a mixing in the x-direction stronger than the corresponding one in the y-direction. This can be better observed in Fig. 4 (corresponding to the same amplitude) where particles initially are evenly distributed all over the basin and each of them is tagged, as indicated in the contours in the first two images on the left. In the upper time sequence, corresponding to an initial gradient in the x-direction, it can be seen that after few cycles regions of positive and negative particles are mixed up, denoting a strong mixing in this direction. On the contrary, a gradient in the y-direction evidences that the upper region of positive particles remains well separated from a lower region of negative particles.

If we now pass to consider the second normal mode shown in Fig. 2b, quite a different behaviour is found. The smaller scale features typical of the second mode are expected to produce a faster chaotic advection, which is in fact observed in Fig. 5 (note that only three cycles are shown compared to nine cycles of the first mode). It is interesting to notice that, especially in the intermediate and large amplitude case, the mixing is now mainly along y, as shown clearly in Fig. 6, where a behaviour in some sense opposite to that of the first normal mode case is evident. Here the evolution of a particle gradient along x evidences two almost disconnected regions (upper sequence), within which a strong mixing along y is present (lower sequence).

Figs. 7 and 8 show the dispersion produced by the flows of Fig. 2c,d respectively. In the mixed first-second mode case (Fig. 7) the dispersion appears to be more isotropic than both the first and the second single modes. When the forcing period is smaller than the lowest eigenperiod (Fig.s 2d and 8) the chaotic advection is limited to the central region where a residual Rossby propagation is present, while in the oscillatory boundary layer no relevant dispersion is found.

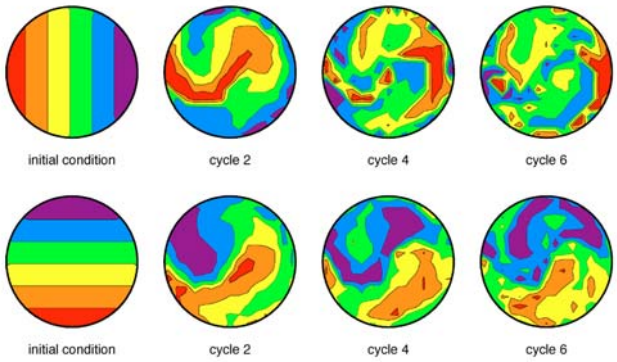

Fig. 4 - Isolines af tagged particles at the initial time, when they are evenly distributed over the basin, and at 2, 4 and 6 cycles for a first-mode basic flow with $\langle|\mathbf{u}|\rangle$=0.05.

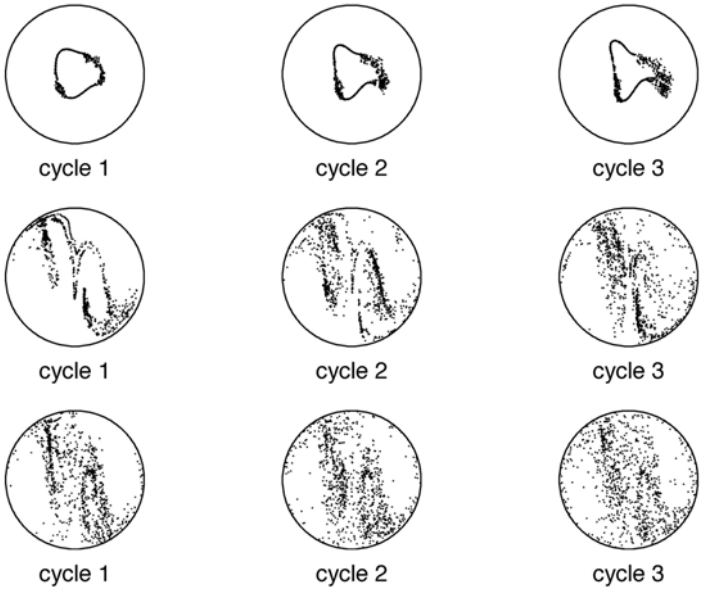

Fig. 5 - Poincaré maps giving the evolved position of 1000 particles initially distributed as in Figure 3. The basic flow is a second normal mode with $\langle|\mathbf{u}|\rangle$=0.01 (upper time sequence), 0.05 (intermediate), 0.1 (lower).

The figures show that, as classically expected, the result of mixing induced by chaotic advection consists of a first phase of stretching and folding of the tracer filaments, during which a strong enhancement of the tracer gradients takes place in the basin, and eventually of a spreading phase of the cluster of particles all over the basin. As underlined by Pierrehumbert (1991), an efficient way to characterize the different stages of mixing is to introduce the particle pair correlation function $H(r)$, defined as the

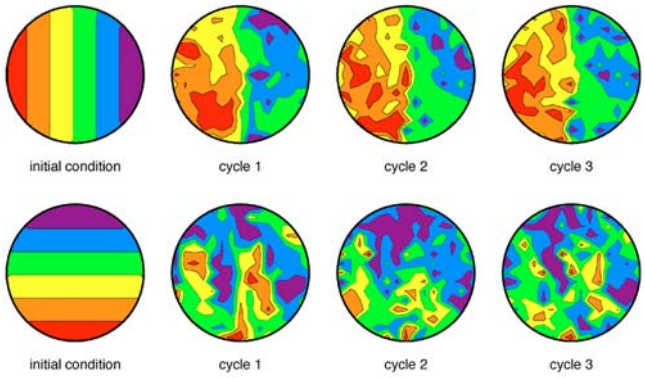

Fig. 6 - Isolines af tagged particles at the initial time, when they are evenly distributed over the basin, and at 1, 2 and 3 cycles for a second-mode basic flow with $\langle|\mathbf{u}|\rangle$=0.05.

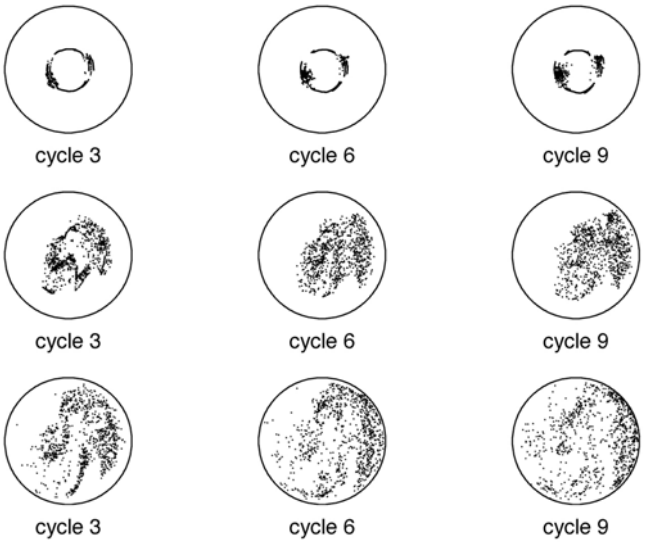

Fig. 7 - Poincaré maps giving the evolved position of 1000 particles initially distributed as in Figure 3. The basic flow is a mixed first-second mode with $\langle|\mathbf{u}|\rangle$=0.01 (upper time sequence), 0.05 (intermediate), 0.1 (lower).

number of particle pairs whose distance, at given times -which we choose to be multiples of the forcing period- is less than *r*. Typically, for a chaotic system $H(r)$ exhibits self-similar subranges in which $H(r) \propto r^{\alpha}$, where α is the correlation dimension (Grassberger and Procaccia, 1983), corresponding to a very compact particle cluster when $\alpha = 0$, to a tracer filament when $\alpha = 1$ and, finally, to a widespread particle cloud when $\alpha = 2$. The computation of *H* in our case confirms that we are looking at a chaotic system. The upper panel of Figure 9 represents the Poincaré maps of a numer-

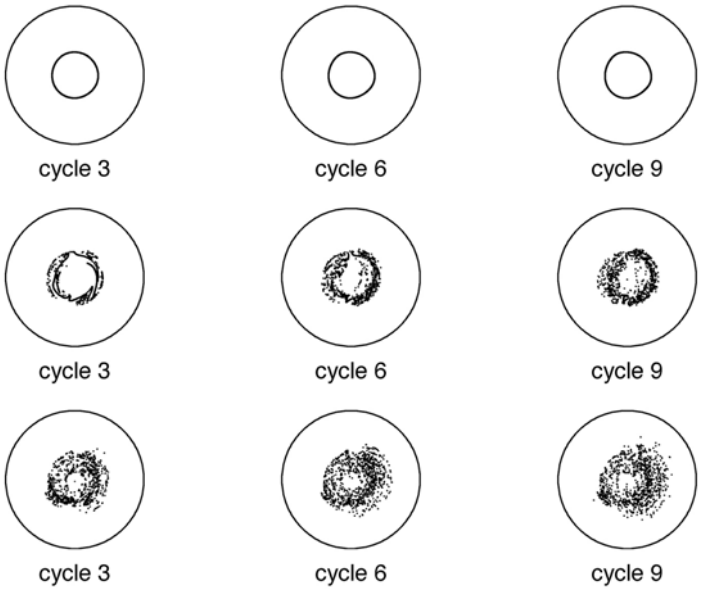

Fig. 8 - Poincaré maps giving the evolved position of 1000 particles initially distributed as in Figure 3. The basic flow is a mixed oscillating boundary layer-first mode with $\langle|\mathbf{u}|\rangle$=0.01 (upper time sequence); 0.05 (intermediate); 0.1 (lower).

ical experiment in which a compact cluster of 100 particles is released in a first-mode basic flow with $\langle|\mathbf{u}|\rangle = 0.1$ (corresponding to the high amplitude case of Figure 3). The evolution of the particle spreading is mirrored by the evolution of the slope of $H(r)$ shown in the lower panel: at the initial time all particles are clustered together, which corresponds to the horizontal line (α=0). As time goes by (note that $H(r)$ is plotted every 2 cycles) its slope grows, passing through the filament stage represented by slopes around α=1 and eventually reaching, after about 15 cycles, the α=2 regime, i.e. that of an area-filling tracer particle cloud. For a smaller amplitude ($\langle|\mathbf{u}|\rangle = 0.05$, Figure 10, corresponding to the intermediate case of Figure 3) 20 cycles are not sufficient for *H* to reach the final regime.

A classical tool used to analyze the effect of chaotic advection is the Maximum Lyapunov Exponent (Lichtenberg and Lieberman, 1982), which represents an estimate of the e-folding time scale of particle pair trajectory divergence:

$$\lambda = \lim_{t\to\infty} \lim_{\delta(0)\to 0} \frac{1}{t} \ln \frac{\delta(t)}{\delta(0)}$$

where δ(t) is the distance between trajectories at time t. Recently, the FSLE (Finite Scale Lyapunov Exponent) has been introduced (Aurell et al., 1997; Artale et al., 1997; see also Boffetta et al., 2000), particularly suitable to study non-asymptotic dispersion processes, thus very appropriate for the study of tracer transport in closed basins, in which the structure of the advecting flow is conditioned by the presence of boundaries (Artale et al., 1997; Lacorata et al., 2001).

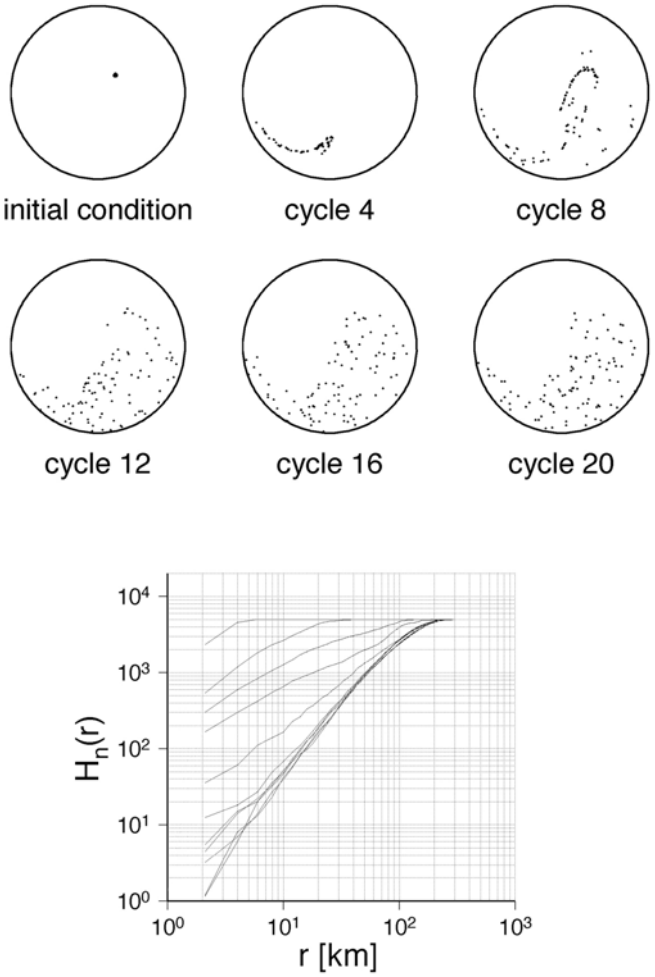

Fig. 9 - Upper panel: Poincaré maps of a numerical experiment in which a compact cluster of 100 particles is released in a first-mode basic flow with $\langle|\mathbf{u}|\rangle$=0.1 The evolution of the particle spreading is mirrored by the slope of the particle pair correlation function $H(r)$(lower panel) reported at every 2 cycles.

The FSLE is defined on the basis of the ensemble average of the "doubling time" τ, i.e. of the time it takes for the separation between particle pairs, initially set at a given value δ, to grow to r $\cdot$ δ, with r > 1 (typically r = 2, whence the definition of τ as doubling time)

$$\lambda(\delta) = \frac{\ln r}{\langle \tau_r(\delta) \rangle}$$

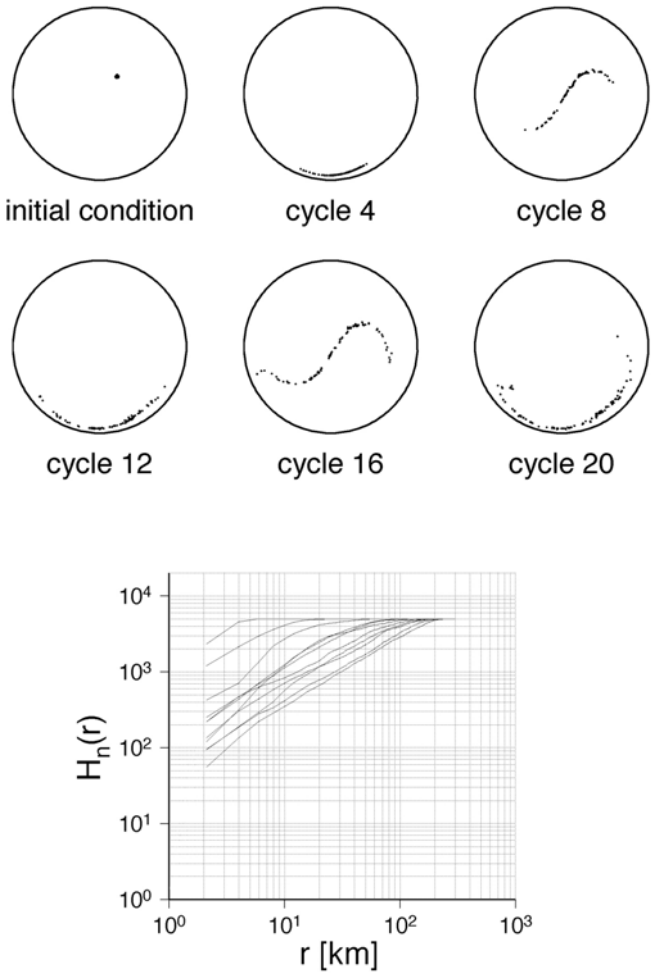

Fig. 10 - Upper panel: Poincaré maps of a numerical experiment in which a compact cluster of 100 particles is released in a first-mode basic flow with $\langle|\mathbf{u}|\rangle$=0.05 The evolution of the particle spreading is mirrored by the slope of the particle pair correlation function $H(r)$ (lower panel) reported at every 2 cycles.

The FSLE has several interesting properties (Boffetta et al., 2000; Lacorata et al., 2001): in particular, in the case of standard diffusion $\lambda(\delta) \sim \delta^{-2}$, and the diffusivity can be estimated as K $\sim \lambda(\delta)\, \delta^2$. A weaker dependence of λ on δ indicates superdiffusive behaviour induced by long time correlations in the advective flow; and a constant value of λ over a broad range of scales indicates exponential trajectory separation.

In figure 11a we show the FSLE for the first mode flow and for three different amplitudes: for the highest amplitude ($\langle|\mathbf{u}|\rangle = 0.1$), $\lambda(\delta)$ is constant over a very broad range of scales, up to O (10 km); for smaller amplitudes, besides attaining lower values, $\lambda(\delta)$ shows a constant behaviour on a smaller range of scales - up to O (1 km) - even though $\lambda(\delta)$ is fairly constant also between the scales 1 to 10 km.

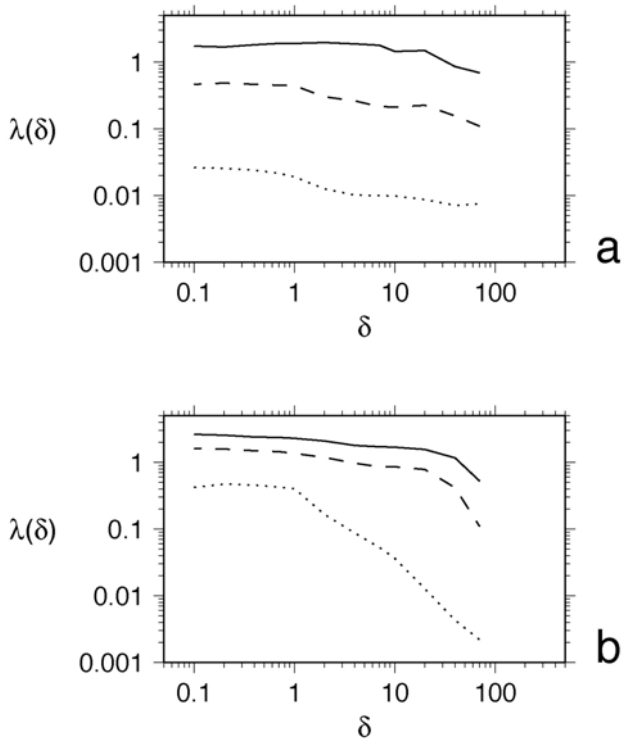

Fig. 11 - Finite Scale Lyapunov Exponent $\lambda(\delta)$ vs δ for: (a) the first Rossby normal mode and for three different amplitudes: $\langle|\mathbf{u}|\rangle$ =0.1 (solid line), $\langle|\mathbf{u}|\rangle = 0.05$ (dashed line), $\langle|\mathbf{u}|\rangle = 0.01$ (dotted line); (b) the second Rossby normal mode and for three different amplitudes: $\langle|\mathbf{u}|\rangle = 1.0$ (solid line), $\langle|\mathbf{u}|\rangle = 0.5$ (dashed line), $\langle|u|\rangle = 0.1$ (dotted line). λ is expressed in days^{-1} and δ in km.

This implies the presence of a pervasive mechanism of chaotic advection, with an induced effective diffusivity which may reach values of the order of a few 10^6 cm^2/s for $\langle|\mathbf{u}|\rangle = 0.1$ for the dimensional case of the Strait of Sicily (see end of Sect. 4), estimating K $\sim \lambda(\delta)\ \delta^2$ taking the highest value for δ in the plateau ($\approx$7 km). Such a value is indeed smaller than those suggested by Okubo (1971) for the diffusivity induced by turbulent diffusion in the upper ocean at scales similar to those of the schematic basin investigated in this work, which is in the range of 10^7 cm^2/s and well agrees with estimates from drifter data in the world ocean (see, e.g., Poulain and Niiler, 1989; Poulain et al., 1996; Bauer et al., 1998; Falco et al., 2000). We obviously expect this to be just one among several different dispersion mechanisms, and yet the above figures show that such effect may well be of non negligible importance in basins characterized by such circulation patterns. As can be deduced from the values plotted in figure 11a, in the case of $\langle|\mathbf{u}|\rangle = 0.05$, K is one order of magnitude less than the above.

The FSLE for the second mode is shown in figure 11b for three different amplitudes. The two modes display different transport characteristics; in particular, the second

mode shows a less widespread presence of exponential separation between trajectories, and clearly approaches a saturation regime which is hampered by the presence of the boundaries. This agrees with the analysis of the Poincaré maps of figure 5, which show a less pronounced stretching and folding and a more diffuse tracer distribution over the basin.

VI. CONCLUSIONS

In this work a general discussion of relevant aspects of planetary and topographic, barotropic and baroclinic Rossby waves and modes based on observational, modeling and laboratory studies in a Eulerian framework is presented. A specific analytical solution of the quasigeostrophic equation of conservation of potential vorticity in terms of Rossby normal modes in a circle is then used to analyze Lagrangian transport properties of Rossby dynamics in a simplified framework.

A relatively simple approach to describe dispersion processes in two-dimensional chaotic flows is that of kinematic models, where the large scale flow is prescribed a priori by assigning a stream function, which may or may not be time-dependent. Even in the latter case, however, the time dependence can be typically removed by a suitable change of coordinates, so that the necessary temporal variability yielding chaotic advection is then to be added in the form of a smaller scale perturbation (see, e.g., Solomon and Gollub, 1988; Pierrehumbert, 1991; Samelson, 1992). The Lagrangian study presented here differentiates itself from previous works in that our large scale flow presents an intrinsic time dependence of modal character yielding chaotic advection, so that no necessity arises of introducing "synthetic" temporal variabilities. In addition, and more importantly, we underline that the choice of the investigated flow, representing Rossby normal modes in a closed basin, is motivated by its strong oceanographic relevance, as discussed in section 3. Therefore, the knowledge of the peculiar dispersion characteristics of Rossby normal modes can be of great importance for deriving diffusivity estimates from in situ data and/or in selecting parametrizations for subgridscale processes to be utilized in numerical simulations.

As could be expected, the presence of Rossby modes inducing velocities with a magnitude comparable to typical speeds observed in ocean subbasins yields indeed dispersion due to chaotic advection. This has been described by means of Poincaré maps and quantified by computing the FSLE for different realizations of the flow, and by constructing particle pair correlation functions. The extension of the present analysis to the case in which the basic flow is produced by an oceanic circulation model rather than provided by an analytical formula, as we have done here, is being carried out.

Acknowledgments

We would like to thank A. Griffa for helpful discussions and A. Vulpiani, who introduced us to the realm of chaos years ago examining our first lagrangian simulations of Rossby normal modes.

[1] Artale, V., G. Boffetta, A. Celani, and A. Vulpiani, 1997: Dispersion of passive tracers in closet basino: Beyond the diffusion coefficient. *Phys. Fluids,* **9**, 3162-3171.
[2] Aurell, E., G. Boffetta, A. Crisanti, G. Paladin and A. Vulpiani, 1997: Predictability in the large: an extension of the concept of Lyapunov exponent. *J. Phys. A*, **30**, 1-26.
[3] Barnier, B., 1984 : Influence of a mid-ocean ridge on wind-driven barotropic Rossby waves. *J. Phys. Oceanogr.,* **14**, 1930-1936.
[4] Bauer, S., M.S. Swenson, A. Griffa, A.J. Mariano and K.Owens, 1998: Eddy-mean flow decomposition and eddy-diffusivity estimates in the tropical Pacific Ocean. Part 1: Methodology *J. Geophys. Res.,* **103**, 30855-30871.
[5] Beardsley, R.C., 1975: The 'sliced-cylinder' laboratory model of the wind-driven ocean circulation. Part 2. Oscillatory forcing and Rossby wave resonance. *J. Fluid. Mech.*, **69**, 41-64.
[6] Boffetta, G., A. Celani, M. Cencini, G. Lacorata, and A. Vulpiani, 2000: Non Asymptotic Properties of Transport and Mixing, *Chaos,* **10,** 50-66.
[7] Candela, J. and Lozano, C.J., 1994: Barotropic response of the western mediterranean to observed atmospheric pressure forcing. In P. La Violette (Editor), *Seasonal and interannual variability of the Western Mediterranean Sea*. Coastal and Estuarine Studies (American Geophysical Union), **46**, 325-359.
[8] Carton, J.A., 1983: The variation with frequency of the long-period tides. *J. Geophys. Res.*, **88**, 7563-7571.
[9] Chao, Y., and L.L. Fu, 1995: A comparison between the TOPEX/POSEIDON data and a global ocean general circulation model during 1992-1993. *J. Geophys. Res.*, **100**, 24,965-24,976.
[10] Chelton, D.B., and M.G. Schlax, 1996: Global observations of oceanic Rossby waves. *Science*, **272**, 234-238.
[11] Cipollini, P., D. Cromwell, G.D. Quartly, and P.G. Challenor, 2000: Remote sensing of oceanic extra-tropical Rossby waves. In "*Satellites, Oceanography and Society*", D. Alpern Editor, Elsevier Science, 99-123.
[12] Crisanti, A., M. Falcioni, G. Paladin, and A. Vulpiani, 1991: Lagrangian chaos: transport, mixing and diffusion in fluids. *Riv. Nuovo Cim.*, **14**, 1-80.
[13] Davis, R.E., 1987: Modelling eddy transport of passive tracers, *J. Marine Res.*, **45**, 635-666.
[14] Döös, K., 1999: Influence of the Rossby waves on the seasonal cycle in the Tropical Atlantic. *J. Geophys. Res.*, **104**, 29,591-29,598.
[15] Falco, P., A. Griffa, P.-M.Poulain and E. Zambianchi, 2000: Transport properties in the Adriatic Sea as deduced from drifter data. *J. Phys. Oceanogr.*, **30**, 2055-2071.
[16] Fu, L.L., and R.A. Davidson, 1995: A note on the barotropic response of sea level to time-dependent wind forcing. *J. Geophys. Res.*, **100**, 24,955-24,963.
[17] Gill, A.E., 1982: *Atmosphere-ocean dynamics*. Academic Press, 662 pp.
[18] Grassberger, P., and I. Procaccia, 1983: Measuring the strangeness of strange attractors. *Physica D*, **9**, 189-208.
[19] Kobashi, F., and H. Kawamura, 2001: Variation of sea surface height at periods of 65-220 days in the subtropical gyre of the North Pacific. *J. Geophys. Res.*, **106**, 26,817-26,831.
[20] Lacorata, G., E. Aurell and A. Vulpiani, 2001: Data analysis and modelling of Lagrangian drifters in the Adriatic Sea,. *Ann. Geophysicae*, **19**, 121-129.
[21] Le Blond, P.H., and L.A. Mysak, 1978: *Waves in the ocean*. Elsevier, 602 pp.
[22] Lichtenberg, A. J., and M.A. Lieberman, 1982: *Regular and Stochastic Motion*, Springer-Verlag.
[23] Luther, D.S., 1982: Evidence of a 4-6 day barotropic, planetary oscillation of the Pacific Ocean. *J. Phys. Oceanogr.,* **12**, 644-657.

[24] Maltrud, M.E., R.D. Smith, A.J. Semtner, and R.C. Malone, 1998: Global eddy-resolving ocean simulations driven by 1985-1995 atmospheric winds. *J. Geophys. Res.*, **103**, 30,825-30,853.
[25] Matano, R.P., 1995: Numerical experiments on the effects of a meridional ridge on the transmission of energy by barotropic Rossby waves. *J. Geophys. Res.*, **100**, 18,271-18,280.
[26] Miller, A.J., D.S. Luther, and M.C. Hendershott, 1993: The fortnightly and monthly tides: resonant Rossby waves or nearly equilibrium gravity waves? *J. Phys. Oceanogr.*, **23**, 879-897.
[27] Miller, A.J., P.F.J. Lermusiaux, and P.M. Poulain, 1996: A topographic-Rossby mode resonance over the Iceland-Faeroe ridge. *J. Phys. Oceanogr.*, **26**, 2735-2747.
[28] Okkonen, S. R., 1993: Observations of topographic planetary waves in the Bering slope current using the Geosat altimeter. *J. Geophys. Res.*, **98**, 22,603-22,613.
[29] Okubo, A., 1971: Oceanic diffusion diagrams. *Deep-Sea Res.*, **48**, 789-802.
[30] Ottino, J.M., 1989: "*The Kinematics of Mixing: Stretching, Chaos and Transport*". Cambridge University Press, (Cambridge) pp. 364.
[31] Pedlosky, J., 1987: *Geophysical Fluid Dynamics*. Springer-Verlag, 710 pp.
[32] Pedlosky, J., 1996: *Ocean Circulation Theory*. Springer-Verlag, 453 pp.
[33] Pedlosky, J., 2000: The transmission of Rossby waves through basin barriers. *J. Phys. Oceanogr.,* **30**, 495-511.
[34] Pedlosky, J., and Greenspan, H.P., 1967: A simple laboratory model for the oceanic circulation. *J. Fluid Mech.,* **27**, 291-304.
[35] Pedlosky, J. and Spall, M., 1999: Rossby normal modes in basins with barriers. *J. Phys. Oceanogr.,* **29**, 2332-2349.
[36] Philander, S.G., 1990: *El Niño, La Niña, and the Southern Oscillation*. Academic Press, 289 pp.
[37] Pierini, S., 1990: A divergent quasi-geostrophic model for wind-driven oceanic fluctuations in a closed basin. *Dyn. Atmos. Oceans*, **14**, 259-277; Corrigendum: **14**, 415.
[38] Pierini, S., 1996: Topographic Rossby modes in the Strait of Sicily. *J. Geophys. Res.*, **101**, 6429-6440.
[39] Pierini, S., 1997: Westward intensified and topographically modified planetary modes. *J. Phys. Oceanogr.*, **27**, 1459-1471.
[40] Pierini, S., 1998a: Modelling studies on the wind-driven dynamics in the Mediterranean Sea. In Proceedings of the *XII Congresso dell'Associazione Italiana di Oceanologia e Limnologia*, 53-63.
[41] Pierini, S., 1998b: Wind-driven fluctuating western boundary currents. *J. Phys. Oceanogr.*, **28**, 2185-2198.
[42] Pierini, 2002a: Sea modeling by microwave altimetry. In "*Remote Sensing of Atmosphere and Ocean from Space: Models, Instruments and Techniques*", *Advances in Global Change Research*, Marzano and Visconti eds., Kluwer Academic Publishers, 165-182.
[43] Pierini, S., 2003: A model of the wind-driven seasonal variability in the tropical North Pacific, with validation through altimeter data. *J. Phys. Oceanogr.*, in press.
[44] Pierini, S., A. Fincham, D. Renouard, R. D'Ambrosio, and H. Didelle, 2002: Laboratory modeling of topographic Rossby normal modes. *Dyn. Atmos. Oceans,* **35**, 205-225.
[45] Pierrehumbert, R.T., 1991: Chaotic mixing of tracer and vorticity by modulated travelling Rossby waves. *Geophys. Astrophys. Fluid Dyn.*, **58**, 285-319.
[46] Platzman, G.W., Curtis, G.A., Hansen, K.S. and Slater, R.D., 1981: Normal modes of the world ocean. Part II: Description of modes in the period range 8 to 80 hours. *J. Phys. Oceanogr.*, **11**, 579-603.
[47] Polito, P.S., and P. Cornillon, 1997: Long baroclinic Rossby waves detected by TOPEX/POSEIDON. *J. Geophys. Res.*, **102**, 3215-3235.
[48] Poulain, P.-M., A. Warn-Varnas and P.P. Niiler, 1996: Near-surface circulation of the Nordic seas as measured by Lagrangian drifters. *J. Geophys. Res.,* **101**, 18237-18258.

[49] Poulain, P.-M., and P.P. Niiler, 1989: Statistical analysis of the surface circulation in the California durrent system using satellite-tracked drifters. *J. Phys. Oceanogr.,* **19**, 1588-1603.
[50] Ripa, P., 1978: Normal Rossby modes of a closed basin with topography. *J. Geophys. Res.*, **83**, 1947-1957.
[51] Robinson, I.S., 1994: *Satellite Oceanography*. Wiley, 455 pp.
[52] Samelson, R.M., 1992: Fluid exchange across a meandering jet. *J. Phys. Oceanogr.*, **22**, 431-440.
[53] Schopf, P.S., D.L.T. Anderson, and R. Smith, 1981: Beta-dispersion of low-frequency Rossby waves. *Dyn. Atmos. Oceans*, **5**, 187-214.
[54] Solomon, T.H., and J.P. Gollub, 1988: Chaotic particle transport in time-dependent Rayleigh-Benard convection. *Phys. Rev.*, A **38**, 6280-6286.
[55] Sommeria, J., Meyers, S.D. and Swinney, H.L., 1991: Experiments on vortices and Rossby waves in eastward and westward jets. In: A.R. Osborne (Editor), *Nonlinear Topics in Ocean Physics*. International School of Physics "Enrico Fermi", Elsevier, **CIX**, 227-269.
[56] Stammer, D., 1997: Steric and wind-induced changes in TOPEX/POSEIDON large-scale sea surface topography observations. *J. Geophys. Res.*, **102**, 20,987-21,009.
[57] Thompson, R. and Luyten, J.R., 1976: Evidence for bottom-trapped topographic Rossby waves from single moorings. *Deep Sea Res.*, **23**, 629-635.
[58] Thompson, R., 1971: Topographic Rossby waves at a site north of the Gulf Stream. *Deep Sea Res.*, **18**, 1-19.
[59] Vivier, F., K.A. Kelly, and L.A. Thompson, 1999: Contributions of wind forcing, waves, and surface heating to sea surface height observations in the Pacific Ocean. *J. Geophys. Res.*, **104**, 20,767-20,788.
[60] White, W.B., 1977: Annual forcing of baroclinic long waves in the tropical North Pacific Ocean. *J. Phys. Oceanogr.*, **7**, 50-61.
[61] White, W.B., Y. Chao, and C.K. Tai, 1998: Coupling of biennial oceanic Rossby waves with the overlying atmosphere in the Pacific basin. *J. Phys. Oceanogr.*, **28**, 1236-1251.
[62] Willebrand, J., S.G.H. Philander, and R.C. Pacanowski, 1980: The oceanic response to large-scale atmospheric disturbances. *J. Phys. Oceanogr.*, **10**, 411-429.
[63] Witter, D.L., and A.L. Gordon, 1999: Interannual variability of South Atlantic circulation from 4 years of TOPEX/POSEIDON satellite altimeter observations. *J. Geophys. Res.*, **104**, 20,927-20,948.
[64] Wunsch, C., 1967: The long-period tides. *Rev. Geophys.*, **5**, 447-475.